*horticulturae*

MDPI

*Article*

# Developing a Hyperspectral Remote Sensing-Based Algorithm to Diagnose Potato Moisture for Water-Saving Irrigation

**Qiqige Suyala [1,2], Zhuoling Li [1], Zhenxin Zhang [3], Liguo Jia [3], Mingshou Fan [3], Youping Sun [4] and Haifeng Xing [1,2,*]**

[1] College of Grassland and Resource Environment, Inner Mongolia Agricultural University, Hohhot 010019, China; imauqiqige@163.com (Q.S.); lzling531@163.com (Z.L.)
[2] Key Laboratory of Agricultural Ecological Security and Green Development at Universities of Inner Mongolia Autonomous, Hohhot 010018, China
[3] College of Agronomy, Inner Mongolia Agricultural University, Hohhot 010018, China; xiaosufine@163.com (Z.Z.); nndjialiguo@163.com (L.J.); fmswh@126.com (M.F.)
[4] Department of Plants, Soils & Climate, Utah State University, Logan, UT 84322, USA; youping.sun@usu.edu
* Correspondence: nmgxinghaifeng@126.com; Tel.: +86-13848812016

**Abstract:** Appropriate water supply is crucial for high-yield and high-quality potato tuber production. However, potatoes are mainly planted in arid and semi-arid regions in China, where the precipitation usually cannot meet the water demand throughout the growth period. In view of the actual situation of water shortage in these areas, to monitor the water status of potato plants timely and accurately and thus precisely control the irrigation are of significance for water-saving management of potatoes. Hyperspectral remote sensing has unique advantages in diagnosing crop water stress. In this paper, the canopy spectral reflectance and plant water content were measured under five irrigation treatments. The spectral parameters that respond to plant water content were selected, and a hyperspectral water diagnosis model for leaf water content (LWC) and aboveground water content (AGWC) of potato plants was established. It was found that potato tuber yield was the highest during the entire growth period under sufficient irrigation, and the plant water content showed a downward trend as the degree of drought intensified. The peak hyperspectral reflectance of potato plant canopies appeared in the red wavelength, where the reflectance varied significantly under different water treatments and decreased with decreasing irrigation. Six models with sensitive bands, first-order derivatives, and moisture spectral indices were established to monitor water content of potato plants. The $R^2$ values of partial least squares regression (PLSR), support vector machine (SVM), and BP neural network (BP) models are 0.8418, 0.9020, and 0.8926, respectively, between LWC and hyperspectral data; and 0.8003, 0.8167, and 0.8671, respectively, between the AGWC and hyperspectral data. These six models can all predict the water content of potato plants, but SVM is the best model for predicting LWC of potato plants. These results are of great significance for guiding precision irrigation of potato plants at different growth stages.

**Keywords:** potato; water diagnosis models; hyperspectral; precision irrigation



**Citation:** Suyala, Q.; Li, Z.; Zhang, Z.; Jia, L.; Fan, M.; Sun, Y.; Xing, H. Developing a Hyperspectral Remote Sensing-Based Algorithm to Diagnose Potato Moisture for Water-Saving Irrigation. *Horticulturae* **2024**, *10*, 811. https://doi.org/10.3390/horticulturae10080811

Academic Editor: Rossano Massai

Received: 17 June 2024
Revised: 29 July 2024
Accepted: 29 July 2024
Published: 31 July 2024



## 1. Introduction

The potato (*Solanum tuberosum* L.) is the fourth most important global food crop after rice, corn, and wheat [1]. In 2020, its planting area and total yield reached 16.49 million hectares and 359.07 million tons, respectively [1]. China is the world's largest potato production country, with a planting area of 5.60 million hectares and a total production of 122.94 million tons in 2020, accounting for 34.24% of the total global production [2]. In terms of planting area, the northern monoculture area has the largest planting area and is the main potato-producing area in China, accounting for more than 50% of the total planting area of potatoes. However, in arid or semi-arid areas, insufficient precipitation cannot meet the water demand of potatoes throughout their entire growing season. Under such water-scarce conditions, precision irrigation is crucial for ensuring high yield, high

quality, and efficient water use of potatoes. Therefore, timely and accurate monitoring of the water status of potatoes and precise irrigation control based on the obtained soil moisture information has practical significance for efficient water management of potatoes.

Hyperspectral technology has become a popular approach for evaluating the vegetation water content due to its fast and convenient operation [3]. When using hyperspectral reflectance to estimate moisture conditions, it is necessary to determine the sensitive bands related to moisture due to the unique spectral characteristics of different compounds. In the original canopy spectral data, the bands at 690 and 740 nm are more suitable for diagnosing plant water conditions [4]. Carter [5] demonstrated that the reflectance sensitivity of leaves to water content is the highest in the spectral bands of 1450, 1950, and 2500 nm. During drought, the near-infrared spectral reflectance of soybean canopy decreases, and the optimal wavelength for detecting water stress is 760–900 nm [6].

The internal water condition of leaves directly reflects the water status of the entire plant [7,8]. Due to the close correlation between leaf water content (LWC) and soil moisture status, soil moisture status reflects the water and fertilizer retention capacity of plants, making it an important indicator of crop moisture status [9]. Thomas et al. [10] discussed the relationship between LWC and infrared spectral reflectance and found a significant negative correlation between them. Tang et al. [11] also reported similar results and pointed out that the spectral reflectance of corn leaves decreased continuously with increasing water content. The relative water content of wheat leaves is positively correlated with the characteristic absorption peak and spectral reflectance area at approximately 1450 nm [12,13]. The relationship between LWC and hyperspectral reflectance varies greatly among different crops, even at different growth stages of the same crop. The correlation between LWC and reflectance in the wavelengths of 810–870 nm and 1480–1650 nm is the highest in the early stage of wheat growth (combining with the booting stage). However, the correlation coefficient of the mature stage (heading–filling–maturity) are even higher in the wavelengths of 1480–1500 and 610–710 nm [14]. Inoue et al. and Yu et al. [15,16] also used reflectance inversion at different wavelengths to calculate the relative water content of canopy leaves. In addition, the first derivative of hyperspectral reflectance is related to LWC [17]. The results of Shibayama and Akiyama [18] showed that the first derivative spectrum at 960 nm is the most sensitive band for predicting rice water status.

After confirming the correlation between plant water status and spectral reflectance using spectral indices and spectral parameters, a hyperspectral-based plant water status monitoring model was constructed. Previous studies have shown that the Normalized Difference Water Index (NDWI) based on the spectral reflectance at 860 nm and 1240 nm wavelengths better reflects plant water content than the NDVI (Normalized Difference Vegetation Index) [19]. NDWI is a normalized ratio index based on the green band and the near-infrared band. It is generally used to get the water body information in images with good effect. Yet, its limitation lies in extracting water bodies with a lot of building backgrounds, such as in cities, while NDVI is closely related to the transpiration of plants, the interception of sunlight, photosynthesis, and the net primary productivity of the surface, etc. It is mainly used to detect the growth status of vegetation, the vegetation coverage, and eliminate some radiation errors, etc. Compared with NDVI, NDWI can effectively obtain the water content information of the vegetation canopy. When the vegetation canopy is under water stress, the NDWI can respond in a timely manner, which is of great significance for monitoring drought. The NDWI and Simple Ratio Index (SR) are also positively correlated with LWC [20]. In addition, Jin et al. [21] found that the Moisture Stress Index (MSI) and Mid-Infrared Vegetation Index (MSVI1) have a close and stable correlation with LWC. The Normalized Difference Spectral Index (NDSI) and Difference Spectral Index (DSI) can predict LWC [22]. Su et al. [23] constructed an optimal monitoring model for plant water content and LWC using the water index (WI), NDWI, MSI, and water band index (WBI). The ratio of WI to NDVI can predict the water contents of the plant and leaves, significantly improving the accuracy of monitoring models [24]. Song [25] conducted nine data transformations on the original spectrum, and then combined

multiple stepwise regression (SMLR), principal component regression (PCR), and partial least squares regression (PLSR) methods to establish a prediction model for LWC of *Populus euphratica*. The PLSR model constructed from the logarithmic reflectance and LWC after the first-order differential change of the original spectrum has the highest accuracy and the best prediction effect. Moreover, Wang et al. [26] constructed an LWC quantitative inversion model for winter wheat based on PLSR by screening the characteristic sensitive bands and calculating spectral indices (NDVI 800 nm, 680 nm; PWI 900 nm, 970 nm; RVI 810 nm, 460 nm, etc.). The neural network method has good predictive ability for crop water content [27]. However, there are relatively few studies that adopt hyperspectral remote sensing and machine learning to study a method to monitor the water status of potato plants in real time.

At present, the hyperspectral estimation of crop LWC is mainly based on a single reflectance index and traditional vegetation indices, and further research is needed to diagnose the multiple combinations of hyperspectral reflectance, derivatives, and moisture index. It is difficult to accurately establish a leaf water monitoring model for the entire growth period of crops using a single vegetation index, and the sensitivity of single-band or fixed-wavelength vegetation indices to crop LWC varies by region, which requires the universality, accuracy, and adaptability of crop water monitoring models. This requires screening the full hyperspectral reflectance band of crop canopy and establishing an estimation model for crop moisture using multiple characteristic parameters such as sensitive bands, derivatives, and water spectral indices. Thus, we conducted research to firstly construct a potato moisture diagnosis model based on hyperspectral characteristic parameters. We carried out experiments with different irrigation amounts during the entire growth period of potatoes. The water status of potato plants was characterized by the water content of leaves. The up-to-date advanced hyperspectral instrument SVC-1024i was used to obtain the hyperspectral data of potato canopies. The characteristic spectral parameters were screened based on the variation patterns of the characterization parameters of plant water content and canopy spectral reflectance during the entire growth period of potatoes. The sensitive bands, the first-order derivative bands, and the water-sensitive index were combined to establish a real-time monitoring model of plant water status during the tuber formation period of potatoes, which is composed of multiple estimation factors. This study is expected to provide a solid and reliable theoretical basis and technical support for the construction of a hyperspectral water diagnosis system for high-yield and efficient potatoes.

## 2. Materials and Methodologies

### *2.1. Plant Materials and Field Experiment under Rainproof Shelters*

The experiments were conducted under rain shelters in Nanshebiya village, Saihan District, Hohhot, Inner Mongolia, China (41°27′ N, 112°63′ E, 1050 m) in 2020–2021. The field soil is chestnut soil (Chinese classification) [28], which contains 15.6 g/kg organic matter, 0.72 g/kg total nitrogen, 38.5 mg/kg available phosphorus (Olsen-P), and 193.7 mg/kg potassium (exchangeable potassium) in 0–60 cm soil layer with a pH of 8.1. The field water capacity (0–60 cm) is 0.2864 g/g. The soil is sandy loam soil; the bulk density and the field water capacity of each soil layer are shown in Table 1.

**Table 1.** The bulk density and water-holding capacity of soil at different depths before sowing.

| | Soil Depth (cm) | | |
|---|---|---|---|
| | **0–20** | **20–40** | **40–60** |
| Bulk density (g/cm$^3$) | 1.47 | 1.50 | 1.53 |
| Water-holding capacity (g/g) | 0.36 | 0.28 | 0.21 |

Two very popular local potato (*Solanum tuberosum* L.) varieties, Kexin No.1 (drought-resistant) and Spunta (drought-sensitive), were planted in 2020 and 2021, respectively. The seed potatoes of the two potato varieties were both provided by Inner Mongolia

Minfeng Seed Industry Co., Ltd. (China). The sowing dates were 10 May 2020, and 12 May 2021. Fertilizer [N (535.65 kg/ha), $P_2O_5$ (375 kg/ha), and $K_2O$ (750 kg/ha)] was applied during sowing. On June 26, plants were top-dressed with urea (488.85 N kg/ha), single superphosphate ($P_2O_5$, 300 kg/ha), and $K_2SO_4$ ($K_2O$, 687.6 kg/ha). The experiment was irrigated by drip irrigation, and the irrigation amount was controlled manually. The drip irrigation tape was double-hole with a spacing of 20 cm. Each treatment was a separate plot. Each plot had an independent water meter and switch, which enabled the irrigation amount to be strictly controlled manually. The five irrigation treatments were as follows: (1) excessive irrigation (EI: 75%, 85%, 95%, and 80% relative soil water content (RSWC) in the seedling, tuber initiation, bulking, and maturation stages, respectively); (2) adequate irrigation (AI: 65%, 75%, 85%, and 70% RSWC, respectively, during the seedling, tuber initiation, bulking, and maturity stages); (3) moderate dehydration (MD: 50%, 60%, 70%, and 55% RSWC, respectively, during the seedling, tuber initiation, bulking, and maturity stages); (4) severe dehydration (SD: 35%, 45%, 55%, and 40% RSWC, respectively, during the seedling, tuber initiation, bulking, and maturation stages); and (5) extreme dehydration (ED: 25%, 35%, 45%, and 30% RSWC, respectively, in the seedling, tuber initiation, bulking, and maturation stages).

$$\text{RSWC (\%)} = (\text{Soil fresh weight} - \text{Soil dry weight})/\text{Soil dry weight} \times 100\% \quad (1)$$

The seedling, tuber initiation, bulking, and maturation stages occur <20 days after emergence (DAE), 20–37 DAE, 38–73 DAE, and >74 DAE, respectively. A completed randomized block design was used with three replicates. The plot size was 6.0 m × 5.6 m, with a row spacing of 0.70 m and a plant spacing of 0.20 m. A two-meter-wide buffer area has been established between the plots to prevent boundary effects and water leakage. Each row was equipped with a drip irrigation pipe, and a solenoid (Hebei YouMite Instrument Manufacturing Co., Ltd., Zhangjiakou, China) was used for irrigation control during each treatment [29]. In all treatments, sufficient water was provided to ensure uniform seedling emergence. After 80% of seedlings appeared, the RSWC was monitored every three days through the oven-drying method. This included sampling the soil at 4:00 pm, oven-drying it overnight, and calculating the irrigation amount for irrigation the next morning. The allowable deviation of RSWC for each treatment was 2% (i.e., the target RSWC for the seedling stage was 75%; if the test value for the 0–60 cm soil layer is less than 73–75%, the irrigation water can reach 77% RSWC). The irrigation quota was calculated as follows based on a previous report [30]:

$$I = 0.6 \times A \times (R_{aim} - R_{test}) \times \rho b \quad (2)$$

where I represents the irrigation quota (t); A represents the irrigated area ($m^2$); $R_{aim}$ represents the RSWC (%); $R_{test}$ represents the tested RSWC (%); and ρb represents the soil bulk density ($g/cm^3$). Under the five water treatments, except for the different irrigation amounts, other soil fertility conditions, soil structure, and fertilization amounts were all the same.

### *2.2. Sampling and Measurements*

During the seedling, tuber initiation, tuber bulking, and maturation stages of potato plants, six plants were harvested from each plot for analysis. After measuring the hyperspectral reflectance of the canopy, leaves, aboveground stems, underground stems, roots, and tubers were separated from the plants, and their fresh weights were measured. Then, the dry weights were measured after they were dried at 105 °C for 30 min and subsequently at 80 °C until they reached a constant weight.

The LWC and AGWC were calculated.

$$\text{AGWC (\%)} = (\text{LFW} + \text{AGSFW}) - (\text{LDW} + \text{AGSDW})/(\text{LFW} + \text{AGSFW}) \quad (3)$$

In Equation (3), LFW represents total leaf fresh weight (g); LDW represents total leaf dry weight (g); AGSFW represents aboveground stem fresh weight; AGSDW represents aboveground stem dry weight.

The determination time of hyperspectral reflectance is consistent with the water content of the plants. The sampling dates for Kexin No. 1 and Spunta were 18, 37, 52, 73, and 90 DAE. Before sampling, the hyperspectral reflectance of the plant canopy was measured using an SVC-1024i Ground Spectrometer (Spectra Vista Corporation, Poughkeepsie, NY, USA) with a working range of 337–2521 nm (Figure 1). On a sunny day with little or no wind, the reflectance at a height of 40–60 cm above the potato plant canopy was measured at 10:00 a.m. and 14:00 p.m. To obtain representative canopy reflectance, five sampling points were selected for each treatment, and 10 spectra images were collected from each sampling point. Then, 50 spectra images were processed and averaged. In addition, during the measurement process, a standard whiteboard was used to promptly correct the "before" and "after" observation results for each group of targets.

**Figure 1.** SVC-1024i Ground Spectrometer.

During the sampling period and each watering period, soil samples were taken using a soil core (diameter: 2.5 cm) at a depth of 0–60 cm to measure RSWC. After drying the soil samples to a constant weight at 105 °C, the RSWC was calculated. RSWC represents the actual soil water content (in percentage), thereby indicating the field water capacity [31]. Soil samples were collected from the midpoint between two seedlings in the planting row, in triplicate for each treatment. Kexin No. 1 and Spunta underwent yield harvesting on 15 September 2020 and 10 September 2021, respectively. The edge row was removed from each processed treatment plot, and the yield was measured using a randomly selected unsampled area of 2 $m^2$.

### *2.3. Hyperspectral Data Processing and Model Construction*

Using MATLAB 2018a (Math Works, Inc., Natick, MA, USA, 2006) (https://www.mathworks.com/products/matlab.html (accessed on 31 May 2024)), the characteristic spectrum of the original band was screened by the successive projections algorithm (SPA). SPA is a forward variable selection algorithm that minimizes collinearity in vector space. Its additional advantage is to extract several characteristic wavelengths of the entire spectrum while eliminating redundancy in the original spectral matrix. The number of selected characteristic bands using SPA is 5–30. The specific steps are as follows: the matrix X (NS, G) is used to represent the most original data, where NS represents the number of samples and G is the dimension of each sample. Initialization: set the number N of variables to be screened; select any column xg from the G column vectors in the matrix as the initial iterative vector. The positions of the unselected column vectors are recorded in the set

M, which can be expressed as Equation (4); calculate the projection of xg on the vectors included in the set T (Equation (5)). Select the column vector with the largest projection as the new projection vector xk (n) and delete it from the set M. Judge the number of selected column vectors at this time. If the number is less than N, it is returned to the second step; otherwise, the calculation is stopped. Set different xk (0) and N, and to obtain circularly different variable sets. Select the best xk (0) and N through the root mean square error (RMSE) of the error analysis graph obtained from the operation.

$$M = \{g, 1 > g > G, g\{k(0), \ldots, k(n), \ldots, k(N-1)\}\} \quad (4)$$

$$Pxg = xg - [xTgxk(n)]\, xk(n)\, [xTk(n)\, xk(n)] - 1 \quad (5)$$

Through correlation analysis, the first-order derivative of reflectance related to the LWC and shoot water content was screened. In addition, 17 spectral indices that are highly sensitive to the plant canopy structure and its water status were selected, and the selected band reflectance, first derivative, and moisture index were combined to form a modeling index library. The main several water spectral indices and their calculation formulas are shown in Table 2.

**Table 2.** Several spectral indices and their algorithm formulas applied in modeling.

| Spectral Index | Formula |
|---|---|
| MSI (Moisture Stress Index) | R1599/R819 |
| NDII (Normalized Difference Infrared Index) | (R819 − R1649)/(R819 + R1649) |
| PSRI (Plant Senescence Reflectance Index) | (R680-R500)/R750 |
| EVI (Enhanced Vegetation Index) | 2.5 × (R800 − R680)/(R800 + 6 × R680 − 7.5R450 + 1) |
| ρr | The minimum band reflectance within the wavelength range of 650 to 690 nm |
| ρg | The maximum band reflectance within the wavelength range of 510 to 560 nm |
| SDr/SDy (Red-edge area/yellow-edge area) | (R780 − R680)/(R640 − R560) |

When building the model, the Kennard–Stone algorithm is used to select training set samples, because the algorithm treats all samples as candidate samples and then sequentially selects them for the training set. First, the two samples with the farthest Euclidean distance were selected as the training set. Then, the Euclidean distance from each remaining sample in the training set to each known sample was calculated, and the candidate samples with the maximum and minimum distances were selected. These samples were then placed into the training set and continued until the required number of samples were reached. PLSR, SVM, and back-propagation neural network (BPNN) methods were used for modeling. The model creation referred to the algorithms and steps reported by Wang et al. [32], Qian et al. [33], and Cheng et al. [34], respectively. A total of 150 sets of hyperspectral data and the corresponding 150 water content data of potato canopy leaves were extracted in this study. The data set was divided into the training set and the test set at a ratio of 7:3. The specific sample division results are shown in Table 3. The accuracy and universality of the constructed model are tested by determining the coefficient ($R^2$) and root mean square error (RMSE). Linear regression on both predicted and measured values was performed, and the slope of the regression model was calculated.

**Table 3.** The sample size of the modeling set and the validation set of PLSR, SVM, and BP regression models.

| | Sample Size | Purpose |
|---|---|---|
| Training set | 105 | modeling |
| Test set | 45 | verify |

### 2.4. Statistical Analyses

The data obtained in this experiment were processed using Microsoft Excel 2013 (Microsoft, Redmond, WA, USA). The analysis of variance was conducted using SPSS18.0 (International Business Machines Corporation, Armonk, NY, USA). Model construction and mapping were performed by self-programming with Matlab 2016 software (Math Works, Natick, MA, USA).

## 3. Results

### 3.1. Yield Response to Different Irrigation Amounts

The maximum yield of Kexin No.1 and Spunta potatoes at harvest reached 82.65 and 58.53 t/ha (Figure 2a,b), respectively. The yield of adequate irrigation (AI) treatment was significantly greater than that of moderate dehydration (MD) treatment throughout the growth stages. However, excessive irrigation (EI), serious dehydration (SD), and extreme dehydration (ED) at the critical growth stage resulted in a decreased potato tuber yield, which is significantly lower than the MD treatment in both cultivars.

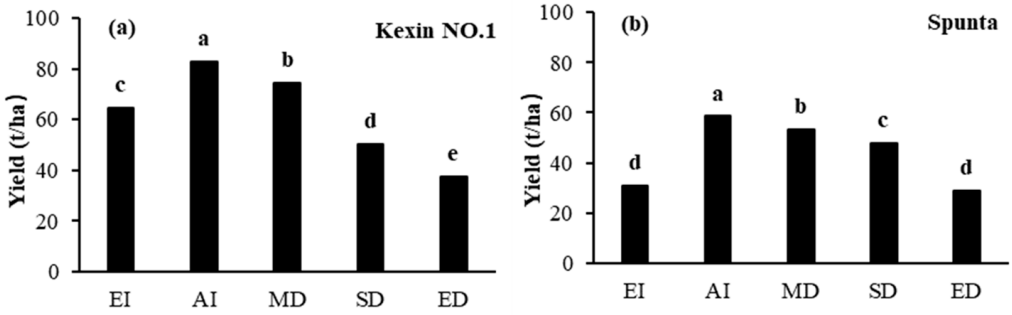


**Figure 2.** Tuber yield at the harvest for potato cultivars (**a**) Kexin No. 1 and (**b**) Spunta under five irrigation treatments. In (**a**,**b**), EI: excessive irrigation treatment, AI: adequate irrigation treatment, MD: moderate dehydration treatment, SD: severe dehydration treatment, ED: extreme dehydration treatment. The tubers with a diameter >0.5 cm were included. The sampling dates are 15 September and 10 September, respectively. Different letters denote statistically significant differences at $p < 0.05$.

### 3.2. Leaf Water Content and Aboveground Water Content

The leaf water content (LWC) of potatoes was reduced under water stress conditions throughout the growth stages. The greater the water stress, the more LWC decreased (Figure 3). The LWC of MD, SD, ED treatments was significantly lower than that of EI and AI treatments. This phenomenon was seen in both cultivars. However, leaf water content under EI treatment was not significantly different from that under AI treatment at 37, 73, and 90 DAE. The consistent results were observed in both Kexin No.1 and Spunta potatoes.

Similar results were observed in aboveground water content (AGWC) of potato plants (Figure 4). Throughout the growth stages, the AGWC was proportional to the soil water content. The AGWC in EI treatment was the highest, followed by AI treatment, although there was no significant difference at 18 and 37 DAE. The AGWC in MD treatment was significantly greater than that in SD treatment, except for 73 and 90 DAE. The AGWC in ED treatment was the lowest in both cultivars.

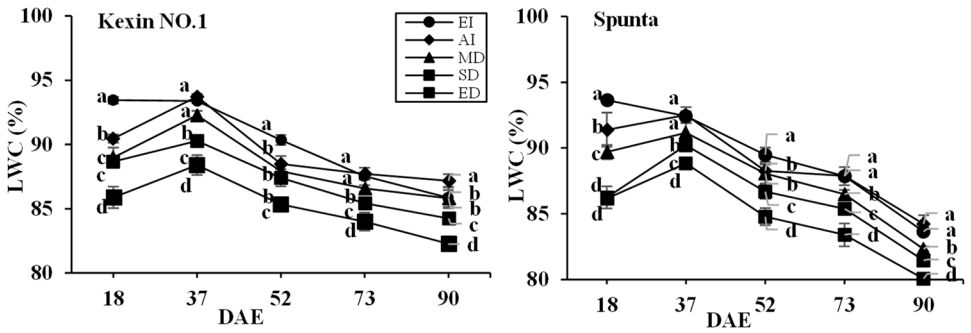


**Figure 3.** The leaf water content of two potato varieties at 18, 37, 52, 73, and 90 days after emergence (DAE) under five irrigation treatments. For the Kexin No.1 (**left**) and Spunta (**right**), EI: excessive irrigation treatment, AI: adequate irrigation treatment, MD: moderate dehydration treatment, SD: severe dehydration treatment, ED: extreme dehydration treatment. (Different lowercase letters in the same column indicate significant differences at the 0.05 level).

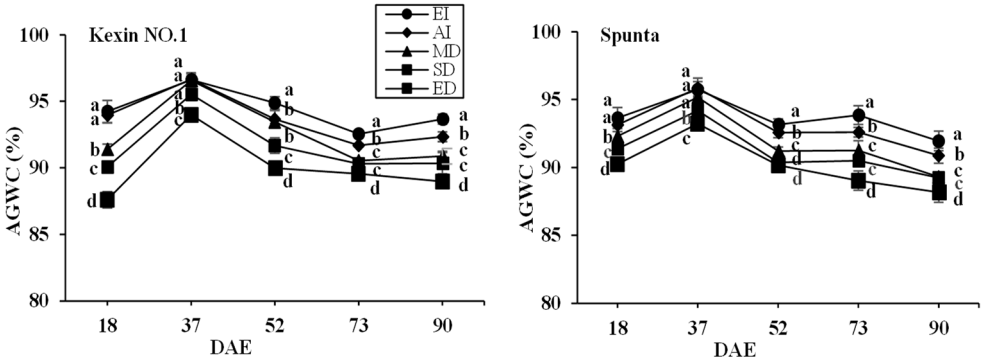


**Figure 4.** The aboveground water content of two potato varieties at 18, 37, 52, 73, and 90 days after emergence (DAE) under five irrigation treatments. For the Kexin No.1 (**left**) and Spunta (**right**), EI: excessive irrigation treatment, AI: adequate irrigation treatment, MD: moderate dehydration treatment, SD: severe dehydration treatment, ED: extreme dehydration treatment. (Different lowercase letters in the same column indicate significant differences at the 0.05 level).

### *3.3. Changes in Hyperspectral Reflectance*

Figure 5a,b show the spectral reflectance of potato plant canopies at different growth stages under water treatments. Although the changes in the spectral reflectance of two potato varieties were consistent under different water treatments, there were variations in spectral reflectance at different growth stages. The spectral reflectance of potato plant canopies in the visible wavelength (400–700 nm) increased initially and then decreased. However, in the 700–1350 nm wavelength, the canopy reflectance significantly increased with increasing irrigation. At 18 and 37 DAE, the spectral reflectance decreased with increasing water stress. In addition, at 52, 73, and 90 DAE, the spectral reflectance of Kexin No. 1 under ED treatment was lower than that of other treatments, whereas the spectral reflectance of ED and SD treatments were lower than that of EI, AI, and MD treatments. In addition, the spectral reflectance of high irrigation treatments was also greater in the 1350–2521 nm wavelength. From Figure 5a,b, it was observed that under water treatments, the spectral reflectance of Kexin No. 1 and Spunta varieties at various growth stages reached their peak values in the red-border region.

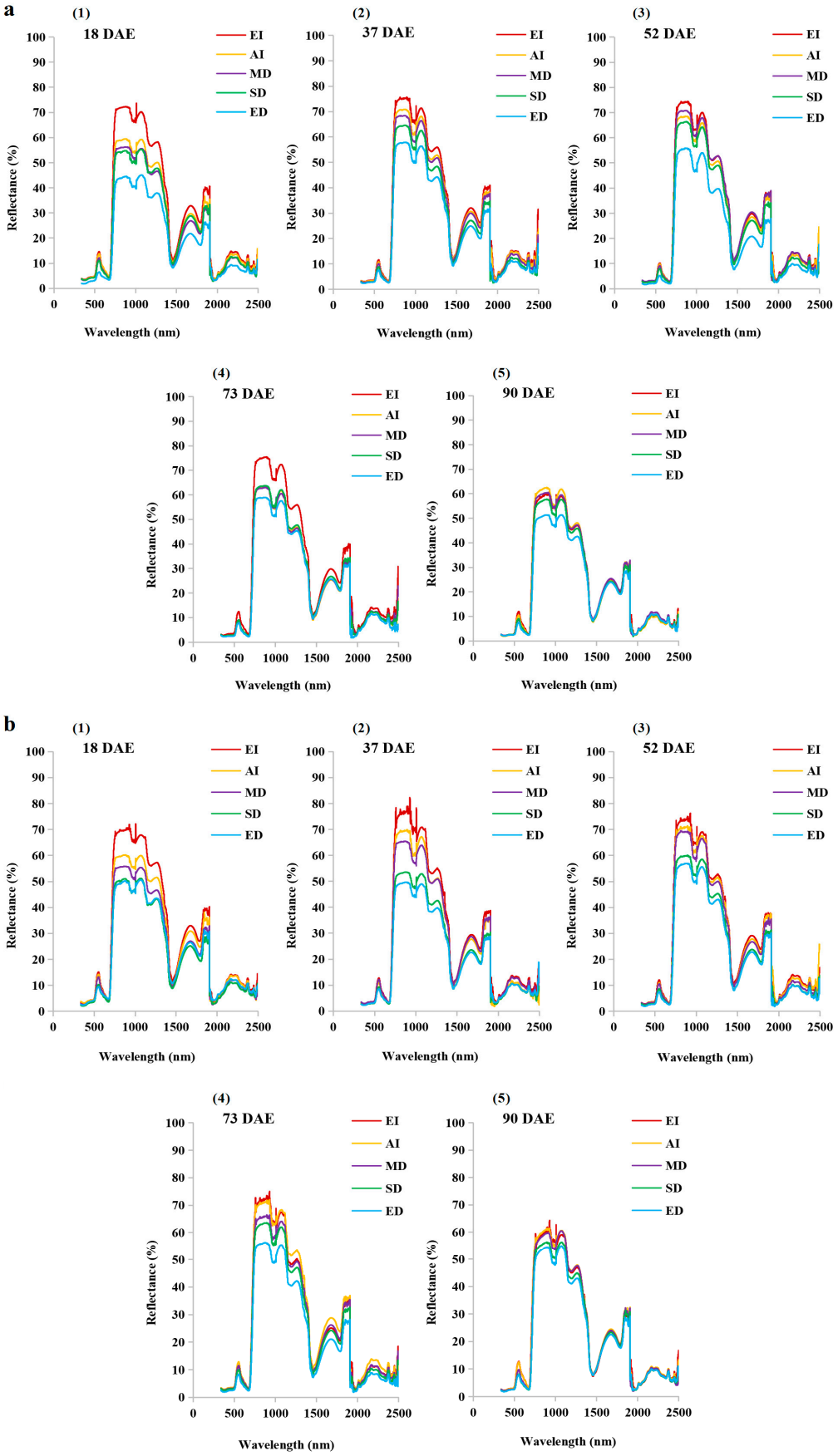


**Figure 5.** Changes in the hyperspectral reflectance under five irrigation treatments for (**a**) Kexin No. 1 and (**b**) Spunta: (1) High spectral reflectance at 337–2521 nm 18 days after emergence (DAE); (2) High

spectral reflectance at 337–2521 nm 37 DAE; (3) High spectral reflectance at 337–2521 nm 52 DAE; (4) High spectral reflectance at 337–2521 nm 73 DAE; (5) High spectral reflectance at 337–2521 nm 90 DAE. In (**a**,**b**), EI: excessive irrigation treatment, AI: adequate irrigation treatment, MD: moderate dehydration treatment, SD: severe dehydration treatment, ED: extreme dehydration treatment.

### *3.4. Hyperspectral Feature Parameters in Relation to Changes in Plant Moisture Status*

Error analysis and sensitive wavelength selection for LWC and AGWC are shown in Figure 6a and 6b, respectively, using the SPA operation program in MATLAB. In the 13th iteration of LWC, when RMSE tends to be stable, 13 sensitive bands including R 725, 856, 1000, 1899, 1915, 1923, 2464, 2473, 2479, 2485, 2490, 2494, and 2499 nm were selected. Among them, there were three bands in the near-infrared wavelength (700–1300 nm) and 10 in the infrared wavelength (1300–2500 nm). In addition, when RMSE tend to be stable in the 16th iteration of AGWC, 16 sensitive bands including R 688, 1001, 1828, 1894, 1901, 1914, 1922, 2282, 2447, 2466, 2475, 2481, 2486, 2491, 2495, and 2498 nm were selected. There were two in the near-infrared wavelength (700–1300 nm) and 14 in the infrared wavelength (1300–2500 nm).

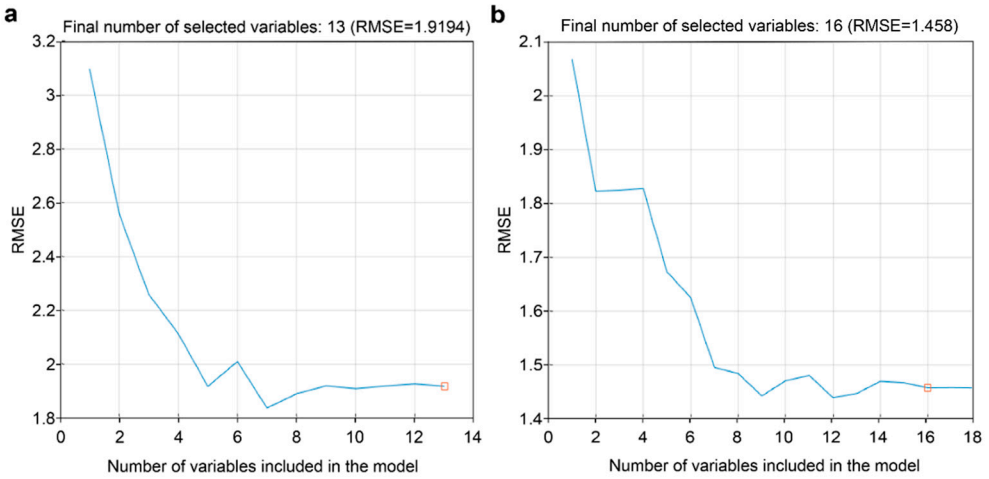


**Figure 6.** The final number of sensitive bands selected when the RMSE value tends to be stable (the curves represent the RMSE value when different numbers of bands were selected): (**a**) LWC, and (**b**) AGWC. The red squares represented the final number of selected variables 13 (**a**) and 16 (**b**) respectively.

Using correlation analysis, we screened the first-order derivatives of reflectance and then selected the first-order derivative with higher correlation coefficients at a probability level of 0.01. The results are shown in Table 4. In addition, we also selected the 17 spectral indices (WBI, NDWI, MSI, NDII, SR, mSR705, PSRI, VOG1, VOG2, VOG3, EVI, NDVI, NDVI705, ρr, ρg, NDρg_ρr, SDr/SDy; among them, NDρg_ρr = (ρg − ρr)/(ρg + ρr), where SDr/SDy represents the ratio of the red-edge area (SDr) and yellow-edge area (SDy)). They are extremely sensitive to the plant water status and together form the indicator basis for establishing the model.

**Table 4.** Correlation analysis between the plant water content index and the first derivative of reflectance.

| Plant Water Content Index | First Derivative of Reflectance | Correlation Coefficient | Plant Water Content Index | First Derivative of Reflectance | Correlation Coefficient |
|---|---|---|---|---|---|
| LWC (%) | D521 | 0.4849 ** | AGWC (%) | D564 | −0.5870 ** |
| | D555 | −0.5731 ** | | D566 | −0.5605 ** |
| | D570 | −0.5307 ** | | D580 | −0.4638 ** |

**Table 4.** *Cont.*

| Plant Water Content Index | First Derivative of Reflectance | Correlation Coefficient | Plant Water Content Index | First Derivative of Reflectance | Correlation Coefficient |
|---|---|---|---|---|---|
| LWC (%) | D521 | 0.4849 ** | AGWC (%) | D564 | −0.5870 ** |
| | D707 | 0.5488 ** | | D603 | −0.4869 ** |
| | D716 | 0.5953 ** | | D712 | 0.5977 ** |
| | D720 | 0.5482 ** | | D1437 | −0.6087 ** |
| | D1519 | 0.6823 ** | | D1464 | 0.6615 ** |
| | D1550 | 0.6242 ** | | D1562 | 0.5755 ** |
| | D1600 | 0.5629 ** | | D1600 | 0.5623 ** |
| | D1810 | 0.4531 ** | | D1810 | 0.5732 ** |
| | D2104 | 0.4426 ** | | D2109 | 0.5116 ** |

**: Represented the first derivative has a higher correlation coefficient at the 0.01 level.

### *3.5. Moisture Monitoring Models*

Partial Least Squares Regression (PLSR)

(1) The regression equation of the spectrum and LWC estimation model is shown as follows:

$$Y = -76.96\,X_1 + 0.9047\,X_2 - 0.4825\,X_3 - 0.2585\,X_4 - 0.0063\,X_5 + 0.0897\,X_6 + 0.0454\,X_7 - 0.1167\,X_8 - 0.1668\,X_9 + 0.0698\,X_{10} - 0.0522\,X_{11} + 0.0801\,X_{12} - 0.0343\,X_{13} - 0.0171\,X_{14} - 37.6423\,X_{15} - 90.3575\,X_{16} + 33.0464\,X_{17} + 3.05611\,X_{18} - 4.0546\,X_{19} + 3.0272\,X_{20} + 69.1098\,X_{21} + 18.1561\,X_{22} + 83.2275\,X_{23} + 24.1908\,X_{24} - 7.7997\,X_{25} + 20.8407\,X_{26} + 80.5652\,X_{27} + 9.9670\,X_{28} - 31.1268\,X_{29} + 0.9602\,X_{30} - 21.5350\,X_{31} - 152.5497\,X_{32} + 77.5729\,X_{33} + 1418.7156\,X_{34} - 1087.3456\,X_{35} - 16.8388\,X_{36} + 71.3621\,X_{37} + 45.8248\,X_{38} + 0.590187\,X_{39} + 0.5798\,X_{40} - 16.1681\,X_{41}$$

where $X_1$ — $X_{13}$, $X_{14}$ — $X_{24}$, and $X_{25}$ — $X_{41}$ represent the sensitive bands, first derivatives, and spectral indices of the indicator library, respectively.

When we extracted 41 components, the ratio of the explanatory dependent variables was 85.21% (Figure 7a), and the modeling effect is better. The $R^2$ = 0.8418, RMSE = 13.0667, and the test set prediction results $R^2$ = 0.6506 of the above PLSR model (Figure 7b).

(2) The regression equation of the spectrum and AGWC estimation model is as follows:

$$Y = 7.0164 - 4.7752\,X_1 - 0.2611\,X_2 + 0.0500\,X_3 + 0.8632\,X_4 - 0.7566\,X_5 - 0.1395\,X_6 - 0.0188\,X_7 - 0.4253\,X_8 + 0.0009\,X_9 - 0.1100\,X_{10} - 0.0567\,X_{11} + 0.1212\,X_{12} + 0.0365\,X_{13} + 0.0657\,X_{14} + 0.0280\,X_{15} - 0.0357\,X_{16} + 41.4394\,X_{17} - 125.7316\,X_{18} + 113.6233\,X_{19} + 58.7286\,X_{20} + 2.5184\,X_{21} + 6.4340\,X_{22} + 33.8752\,X_{23} - 15.3368\,X_{24} + 52.1277\,X_{25} + 1.9704\,X_{26} + 12.0724\,X_{27} - 0.6198\,X_{28} + 89.3110\,X_{29} + 23.6743\,X_{30} - 19.3636\,X_{31} - 0.3763\,X_{32} + 7.1523\,X_{33} - 103.3082\,X_{34} + 59.9540\,X_{35} + 1.1573\,X_{36} + 133.4231\,X_{37} - 11.4335\,X_{38} + 89.1469\,X_{39} - 119.7034\,X_{40} + 8.9216\,X_{41} - 0.0983\,X_{42} + 31.8028\,X_{43} - 17.1274\,X_{44}$$

Among them, $X_1$ — $X_{16}$, $X_{17}$ — $X_{27}$, and $X_{28}$ — $X_{44}$ represent the sensitive bands, the first derivatives, and the spectral indices of the indicator library, respectively.

When we extracted the 44 components, the ratio of the explained dependent variables was 80.03% (Figure 8a). $R^2$ = 0.8003, RMSE = 10.3801, and the test set prediction results $R^2$ = 0.5972 of the above PLSR model (Figure 8b).

### *3.6. Support Vector Machine (SVM)*

The results of the SVM-based LWC prediction model are as follows: The training set was trained, and the training results are shown in Figure 9a. The training set $R^2$ is 0.9020, and the test set $R^2$ is 0.6432. The results of the SVM-based AGWC prediction model are as follows: The training set was trained, and the training results are shown in Figure 9b; the training set $R^2$ is 0.8167 and the test set $R^2$ is 0.6876.

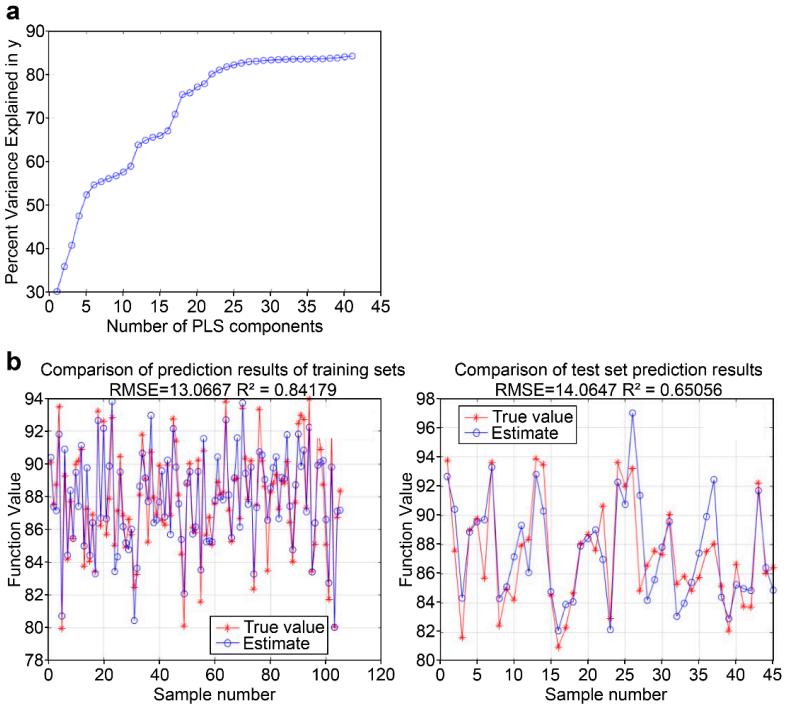


**Figure 7.** Percentage of the principal component contribution: the explanatory degree of 41 partial least squares components to y (**a**) and the fitting effect of the regression model between the hyperspectral reflectance and leaf water content (LWC): RMSE and $R^2$ of the training set (**bottom left**) and the test set (**bottom right**), respectively (**b**).

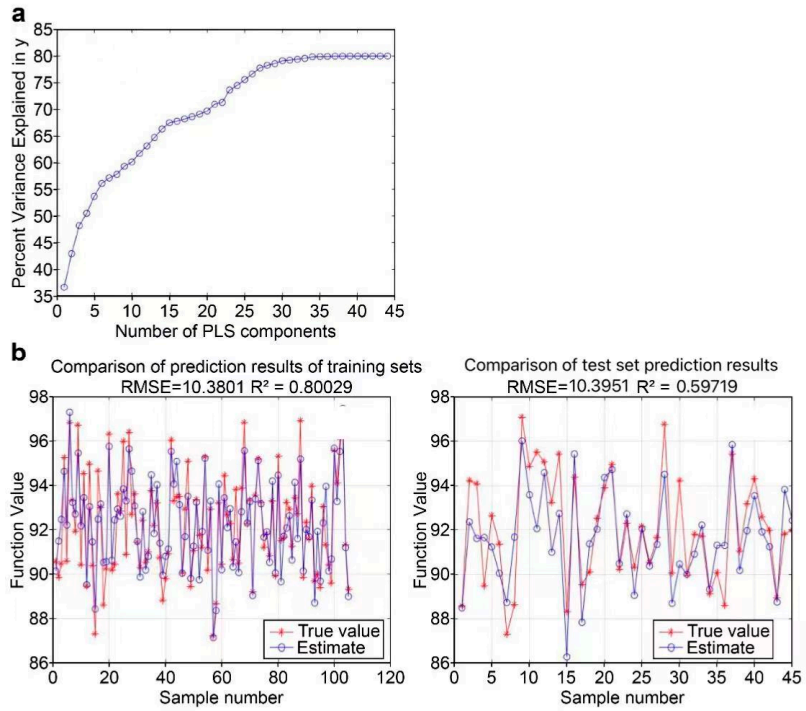


**Figure 8.** Percentage of the principal component contribution: the explanatory degree of 44 PLS components to y (**a**) and the fitting effect of the regression model between the hyperspectral reflectance and aboveground water content (AGWC): RMSE and $R^2$ of the training set (**bottom left**) and the test set (**bottom right**), respectively (**b**).

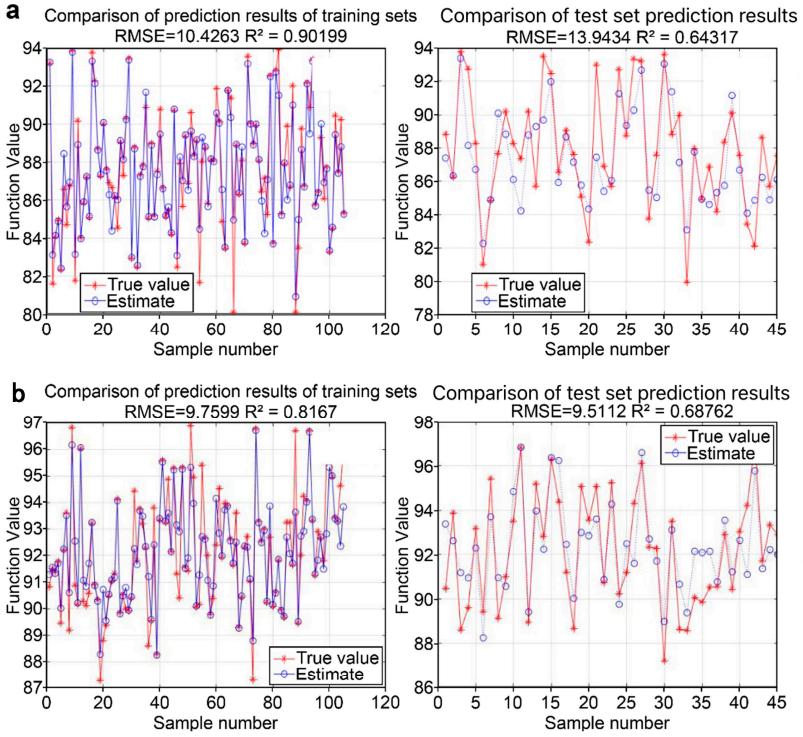


**Figure 9.** Fitting hyperspectral reflectance with leaf water content (LWC) and aboveground water content (AGWC) using SVM (support vector machine) regression models: (**a**) LWC, prediction results of training set (**top left**) and test set (**top right**); (**b**) AGWC, prediction results of training set (**bottom left**) and test set (**bottom right**).

### *3.7. Back-Propagation Neural Network*

A range of 8–16 hidden nodes were selected for the experiment. Table 5 shows that LWC and AGWC have the best model fit, with 12 hidden nodes. For this hidden node, the model fit $R^2$ of the BP neural network regression model between the spectrum and LWC is 0.8926, while that of $R^2$ between the spectrum and AGWC is 0.8671 (Figure 10a,b).

**Table 5.** The $R^2$ values of different hidden nodes screened by the back-propagation neural network models of leaf water content (LWC) and aboveground water content (AGWC).

| Plant Water Content Index | Number of Hidden Nodes | $R^2$ | Plant Water Content Index | Number of Hidden Nodes | $R^2$ |
|---|---|---|---|---|---|
| LWC (%) | 8 | 0.8499 | AGWC (%) | 8 | 0.7393 |
| | 9 | 0.8395 | | 9 | 0.7264 |
| | 10 | 0.8707 | | 10 | 0.7484 |
| | 11 | 0.7620 | | 11 | 0.7964 |
| | 12 | 0.8926 | | 12 | 0.8671 |
| | 13 | 0.8466 | | 13 | 0.6822 |
| | 14 | 0.8453 | | 14 | 0.7532 |
| | 15 | 0.8338 | | 15 | 0.6901 |
| | 16 | 0.7959 | | 16 | 0.8303 |

In summary, through comparative analysis, PLSR, SVM, and BP models have a higher model fit on LWC than on AGWC, with $R^2$ values reaching 0.8418, 0.9019, and 0.8926, respectively. This indicates that the potato LWC monitoring model based on hyperspectral data has high accuracy for prediction. When using three models to predict potato LWC, the $R^2$ values were as high as 0.8193, 0.9192, and 0.7538 (Figure 11). This further indicates that using SVM based on hyperspectral data to estimate potato LWC is the best choice.

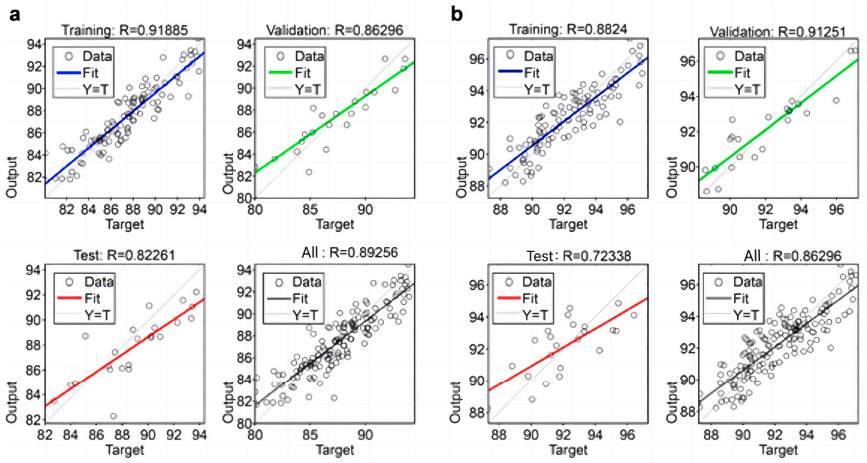


**Figure 10.** Fitting hyperspectral reflectance with the LWC and AGWC of potato plants using back-propagation neural network regression models. (**a**) LWC, the training set (**top left**), the test set (**bottom left**), the validation set (**top right**), and the overall result (**bottom right**); (**b**) AGWC, the training set (**top left**), the test set (**bottom left**), the validation set (**top right**), and the overall result (**bottom right**).

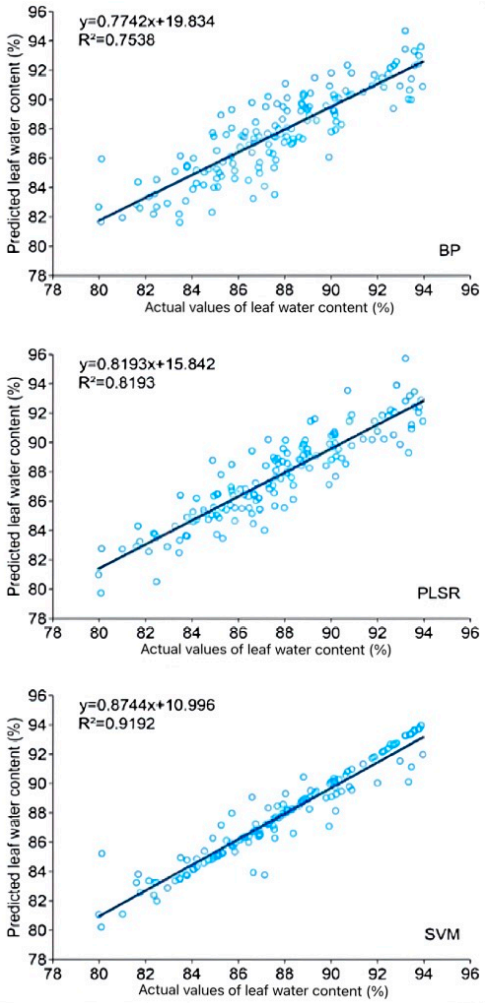


**Figure 11.** Comparison of the prediction models of potato leaf water content (LWC) obtained through BP (**top**), PLSR (**middle**), and SVM (**bottom**) models. The figure contains a quantity of 150 samples. Black straight lines represent the linear relationship between the predicted leaf water content and the measured leaf water content.

## 4. Discussion

As a result of global climate change and population growth, freshwater shortage has become increasingly serious. Agriculture is a major water consumer, so water conservation from irrigation in agriculture has great potential. Precision irrigation, recognized as a superior method to traditional irrigation in recent years, aims to achieve precise control and supply of water through scientific management and technical means according to the actual needs of crop growth. Among these methods, drip irrigation directly delivers water to the roots of crops through pipelines, achieving a high water utilization rate. This saves water resources and reduces weed growth. To accelerate the promotion and application of precision irrigation technology, the Chinese government has taken a series of measures. For example, the government supports scientific research institutes and enterprises in the research and development of precision irrigation technology. It also encourages farmers to adopt precision irrigation technology by increasing investment in technology research and development, providing government guidance, and offering financial subsidies. In Xinjiang, for example, the local government has vigorously promoted precision irrigation technology, achieving remarkable results. The adoption of drip irrigation in cotton planting not only saves water resources but also improves yield and quality.

Potatoes require significant water during the growth period, so research on their precise irrigation is crucial.

Studies have shown that drought inhibits potato growth leading to yield reduction. Water stress decreases plant height and tuber yield by reducing the number of stolons per plant [35,36]. With increased stress, the growth rate of potatoes significantly decreases, affecting leaf expansion, plant elongation, and overall crop yield. The responses of potatoes to water deficit varies at different growth periods. Water stress during the tuber expansion period significantly reduces potato yield to 28,633.3 kg/hm$^2$, 18.93% lower than under full irrigation [37]. However, appropriate water stress can improve water use efficiency and potato quality, ensuring minimal yield reduction and supporting sustainable agriculture.

The regulation of water conditions directly affects the quality and yield of potato tubers. Therefore, it is essential to monitor the water content of potato leaves or aboveground parts quickly and accurately. Canopy hyperspectral measurement is a simple, fast, nondestructive method with a wide range of spectral indicators, making it suitable for quickly estimating field water content. The quantitative relationship between canopy spectral reflectance and LWC and AGWC shows improved correlation in the near-infrared region, which is consistent with the results of Carter [5] and Cibula et al. [38]. In this study, the 400–2500 nm band was selected for analysis. The sensitive wavelengths extracted through the SPA method, which reduces data dimension and improves modeling speed, align with those proposed by previous researchers [39]. Based on this, the feasibility of using hyperspectral parameters to diagnose potato water status was assessed, leading to the development of three water diagnosis models, PLSR, SVM, and BP, for precise water management during the critical growth period.

Due to strong reflection on fresh leaves and structural influences, estimating crop water status using a single spectral reflectance is challenging. However, constructing spectral indices enhances the utilization of effective spectral information on vegetation, reduces external influences, and improves the accuracy of prediction models [40]. Peñuelas and Inoue [24] improved the prediction accuracy of LWC by establishing spectral indices such as WI (900, 970) and WI to NDVI ratio index (900, 680). Yu et al. [16] proposed the spectral index RSI (2200, 1430) for monitoring the water status of grasses and woody plants. In this study, we applied the previously proposed water sensitivity spectral index [41–43], combined with sensitivity bands and first derivatives, to establish an LWC diagnosis model. The results showed that expanding the spectral index range and introducing mixed characteristic spectral parameters improved the prediction performance of crop LWC, with $R^2 > 0.6$. The hyperspectral prediction model of potato LWC also showed good stability.

Although potato canopy hyperspectral data were used in this study, selecting sensitive bands, the first derivative of reflectance, and spectral indices, and then establishing esti-

mation models of potato leaf and aboveground water content based on machine learning algorithms using combined characteristic parameters, can achieve good prediction results. However, there are still shortcomings: the sensitive bands and indices of potato leaf water content may vary at different growth stages, and the characteristic spectral parameters of the constructed model may change. Further canopy leaf water and hyperspectral data collection at each growth stage is necessary to verify and correct the potato water estimation model, improving the universality and practicality.

## 5. Conclusions

Adequate water supply throughout the growth period is necessary to achieve a high yield of potato tubers. The LWC and AGWC were higher under treatments with larger irrigation amounts compared to water stress treatments. Under different water supply conditions, the hyperspectral reflectance trends of these two potato varieties over the two years are similar. It is worth noting that the reflection peaks appeared at 700, 1800, and 2400 nm, with significant differences in the hyperspectral reflectance between different irrigation treatments in the ranges of 700–1100 nm, 1800–1950 nm, and 2400–2500 nm. This suggests that estimating the water content of potato plants using hyperspectral methods is feasible. The accuracy of the PLSR, SVM, and BP prediction models established between LWC and hyperspectral characteristic parameters was higher than that of AGWC. Among these, the SVM model had the highest prediction accuracy for leaf moisture content, with an $R^2$ value of 0.9020.

In subsequent studies, selecting the optimal spectral monitoring parameters for characterizing LWC at different stages of potato growth will be the preferred method. Based on this, high-precision monitoring models for leaf water content of potatoes at various growth periods will be further established. Additionally, this study was conducted in the Inner Mongolia region of China, which has a temperate continental climate. The soil type in the potato planting area is sandy loam. The gradient treatment of irrigation amounts involved different percentages of the maximum field capacity of water during each growth period of potatoes, representing varying degrees of drought, sufficiency, and waterlogging. It is necessary to expand the water content range of potato plants for specific climate areas to enhance the monitoring adaptability of the model. Both Kexin No. 1 and Spunta are medium-late maturing potato varieties. Further research on the normalized water diagnosis of potato varieties with different maturity periods is required to validate the practicality of the established model.

**Author Contributions:** Conceptualization, M.F.; Methodology, Q.S., L.J., Y.S. and H.X.; Formal analysis, Z.L.; Data curation, Y.S. and H.X.; Writing—original draft, Q.S., Z.L. and Z.Z.; Writing—review & editing, L.J. and H.X.; Supervision, M.F.; Project administration, Q.S. and H.X.; Funding acquisition, Q.S. and H.X. All authors have read and agreed to the published version of the manuscript.

**Funding:** The research is financed by the National Natural Science Foundation of China (31960388), Natural Science Foundation of Inner Mongolia (2023LHMS03046, 2018BS03002), Science and Technology Planning Project of Inner Mongolia (RZ2300000133) and the research start-up funds of IMAU (NDYB2017-19).

**Data Availability Statement:** The original contributions presented in the study are included in the article, further inquiries can be directed to the corresponding author.

**Conflicts of Interest:** The authors have no conflicts of interest to declare.

## References

1. Available online: http://www.fao.org/faostat/en/#data/QCL (accessed on 21 March 2024).
2. Luo, Q.; Gao, M.; Liu, Z.; Lu, H.; Zhang, S. Analysis on the development situation of Chinese potato industry in 2020. In *Malingshu Chanye Yu Lvse Fazhan, Proceedings of the 23rd China Potato Conference in 2021, Yulin, Shaanxi, 24 July 2021*; Heilongjiang Science and Technology Press: Harbin, China, 2021; (In Chinese with English Abstract). [CrossRef]
3. Tang, Y.; Huang, J. Study on hyperspectral remote sensing in agriculture. *Remote Sens. Technol. Appl.* **2001**, *16*, 248–251.

4. Dobrowski, S.; Pushnik, J.; Zarco-Tejada, P.J.; Ustin, S.L. Simple reflectance indices track heat and water stress-induced changes in steady-state chlorophyll fluorescence at the canopy scale. *Remote Sens. Environ.* **2005**, *97*, 403–414. [CrossRef]
5. Carter, G.A. Primary and secondary effects of water content on the spectral reflectance of leaves. *Am. J. Bot.* **1991**, *78*, 916–924. [CrossRef]
6. Holben, B.N.; Schutt, J.B.; McMurtrey, J., III. Leaf water stress detection utilizing thematic mapper bands 3, 4 and 5 in soybean plants. *Int. J. Remote Sens.* **1983**, *4*, 289–297. [CrossRef]
7. Walthall, C.; Dulaney, W.; Anderson, M.; Norman, J.; Fang, H.; Liang, S. A comparison of empirical and neural network approaches for estimating corn and soybean leaf area index from Landsat ETM+ imagery. *Remote Sens. Environ.* **2004**, *92*, 465–474. [CrossRef]
8. Borzuchowski, J.; Schulz, K. Retrieval of leaf area index (LAI) and soil water content (WC) using hyperspectral remote sensing under controlled glass house conditions for spring barley and sugar beet. *Remote Sens.* **2010**, *2*, 1702–1721. [CrossRef]
9. Huo, H.; Zhang, Y.; Chen, L.; Li, C.; Gao, H. Physiological response and evaluation of drought resistance about five desert shrubs under drought stress. *J. Arid. Land Resour. Environ.* **2011**, *25*, 185–189. [CrossRef]
10. Thomas, J.; Namken, L.; Oerther, G.; Brown, R. Estimating leaf water content by reflectance measurements. *Agron. J.* **1971**, *63*, 845–847. [CrossRef]
11. Tang, Y.; Huang, J.; Wang, X.; Wang, R.; Wang, F. Comparison of the characteristics of hyperspectra and red edge in rice, corn and cotton. *Sci. Agric. Sin.* **2004**, *1*, 29–35. [CrossRef]
12. Tian, Q.; Gong, P.; Zhao, C.; Guo, X. The feasibility of using spectral reflectance to diagnose wheat moisture status was analyzed. *Chin. Sci. Bull.* **2000**, *45*, 6, (In Chinese with English Abstract). [CrossRef]
13. Wang, J.; Zhao, C.; Guo, X.; Tian, Q. Study on the water status of the wheat leaves diagnosed by the spectral reflectance. *Sci. Agric. Sin.* **2001**, *34*, 104–107. [CrossRef]
14. Tian, Y.; Zhu, Y.; Cao, W.; Dai, T. Relationship between canopy reflectance and plant water status of wheat. *Chin. J. Appl. Ecol.* **2004**, *11*, 2072–2076, (In Chinese with English Abstract).
15. Inoue, Y.; Morinaga, S.; Shibayama, M. Non-destructive estimation of water status of intact crop leaves based on spectral reflectance measurements. *Jpn. J. Crop Sci.* **1993**, *62*, 462–469. [CrossRef]
16. Yu, G.R.; Miwa, T.; Nakayama, K.; Matsuoka, N.; Kon, H. A proposal for universal formulas for estimating leaf water status of herbaceous and woody plants based on spectral reflectance properties. *Plant Soil* **2000**, *227*, 47–58. [CrossRef]
17. Danson, F.; Steven, M.; Malthus, T.; Clark, J. High-spectral resolution data for determining leaf water content. *Int. J. Remote Sens.* **1992**, *13*, 461–470. [CrossRef]
18. Shibayama, M.; Akiyama, T. Seasonal visible, near-infrared and mid-infrared spectra of rice canopies in relation to LAI and above-ground dry phytomass. *Remote Sens. Environ.* **1989**, *27*, 119–127. [CrossRef]
19. Gao, B.C. NDWI—A normalized difference water index for remote sensing of vegetation liquid water from space. *Remote Sens. Environ.* **1996**, *58*, 257–266. [CrossRef]
20. Zhao, J.; Li, J.; Zhang, C.; Du, S.; Yao, Y.; Wang, Q.; Zhao, S. Estimating and validating wheat leaf water content with three MODIS spectral indexes: A case study in Ningxia Plain. *China. J. Agric. Sci. Technol.* **2018**, *18*, 387–398.
21. Jin, L.; Li, Y.; Xu, D.; Guo, J.; Zhang, B. Spectroscopy diagnostics of water content and greenness features in wheat leaf. *Chin. J. Agrometeorol.* **2012**, *33*, 124–128. [CrossRef]
22. Liu, X.J.; Tian, Y.C.; Yao, X.; Cao, W.X.; Zhu, Y. Monitoring leaf water content based on hyperspectra in rice. *Sci. Agric. Sin.* **2012**, *45*, 435–442. [CrossRef]
23. Su, Y.; Wang, K.; Li, S.; Xiao, C.; Chen, B.; Wang, F.; Tang, Q.; Chen, J.; Jin, X.; Lu, Y.; et al. Monitoring models of the plant water content based on cotton canopy hyperspectral reflectance. *Cotton Sci.* **2010**, *22*, 554–560.
24. Peñuelas, J.; Inoue, Y. Reflectance indices indicative of changes in water and pigment contents of peanut and wheat leaves. *Photosynthetica* **1999**, *36*, 355–360. [CrossRef]
25. Song, Y. Analysis on Characteristics of Desert Adult *Populus euphratica* Leaves Water Content in Spring Using Ground Hyperspectral Data. Master's Thesis, Xinjiang University, Ürümqi, China, 2015. (In Chinese with English Abstract).
26. Wang, Y.; Zhang, X.; Jin, Y.; Gu, X.; Feng, H.; Wang, C. Quantitative retrieval of water content in winter wheat leaves based on continuous wavelet transform. *J. Triticeae Crops* **2020**, *40*, 503–509, (In Chinese with English Abstract).
27. Zhang, Y.; Fu, L.; Zhou, X. Near infrared detection of wheat water content based on BP neural network. *J. Henan Univ. Technol.* **2013**, *34*, 17–20. [CrossRef]
28. Cui, Z.; Fan, R.; Li, S.; Zhang, S. Major characteristics and rational utilization of chestnut soil of Inner Mongolia. *J. Arid. Land Resour. Environ.* **1990**, *4*, 25–30.
29. Wang, J.; Yang, J.; Cai, J.; Zhai, G. Experimental study on the influence of working pressure and spraying angle on the single-hole spray characteristics of micro-sprinkling hose. *Water Sav. Irrig.* **2018**, *3*, 35–38.
30. Ahmadi, S.H.; Andersen, M.N.; Plauborg, F.; Poulsen, R.T.; Jensen, C.R.; Sepaskhah, A.R.; Hansen, S. Effects of irrigation strategies and soils on field grown potatoes: Yield and water productivity. *Agric. Water Manag.* **2010**, *97*, 1923–1930. [CrossRef]
31. Rab, M.; Chandra, S.; Fisher, P.; Robinson, N.; Kitching, M.; Aumann, C.; Imhof, M. Modelling and prediction of soil water contents at field capacity and permanent wilting point of dryland cropping soils. *Soil. Res* **2011**, *49*, 389–407. [CrossRef]
32. Wang, G.; Ye, H. *Principal Component Analysis and Partial Least Squares Method*; Tsinghua University Press: Beijing, China, 2012; ISBN 978-7-302-27942-6.

33. Cheng, J.; Xu, J.; Wang, Y.; Zhang, H.; Li, X. Granary rice temperature prediction model based on BP neural network. *Mod. Electron. Tech.* **2021**, *44*, 5, (In Chinese with English Abstract). [CrossRef]
34. Qian, F.; Jiang, W.; Che, Z.; Gan, J. Application of PSO-SVM alogrithm in modeling of temperature control system at metro station. *Urban Mass Transit Res.* **2014**, *17*, 86–89, (In Chinese with English Abstract). [CrossRef]
35. Rahaman, E.H.M.S.; Khan, M.S.A.; Bazzaz, M.M. Plant canopy, tuber yield and growth analysis of potato under moderate and severe drought condition. *J. Plant Sci.* **2014**, *2*, 201–208. [CrossRef]
36. Zhao, H.; Xiong, Y.; Li, F.; Wang, R.; Qiang, S.; Yao, T.; Mo, F. Plastic film mulch for half growing-season maximized WUE and yield of potato via moisture-temperature improvement in a semi-arid agroecosystem. *Agric. Water Manag.* **2011**, *104*, 68–78. [CrossRef]
37. Zhang, W.; Zhang, H.; Li, F.; Wang, Z.; Gao, J.; Ba, Y. Effects of regulated drip irrigation at different growth stages on yield, quality and water use efficiency of potato in Oasis Region. *Acta Agric. Boreali-Sin.* **2019**, *34*, 145–152. [CrossRef]
38. Cibula, W.G.; Zetka, E.F.; Rickman, D.L. Response of thematic mapper bands to plant water stress. *Int. J. Remote Sens.* **1992**, *13*, 1869–1880. [CrossRef]
39. Pan, Q.; Zhang, J.; Zhang, J. Analysis of correlation and differences between leaf moisture and hyperspectral reflectance among different walnut varieties. *For. Res.* **2019**, *32*, 1–6.
40. Cheng, T.; Rivard, B.; Sánchez-Azofeifa, A. Spectroscopic determination of leaf water content using continuous wavelet analysis. *Remote Sens. Environ.* **2011**, *115*, 659–670. [CrossRef]
41. Hunt, E.R.; Rock, B.N. Detection of changes in leaf water content using near- and middle-infrared reflectances. *Remote Sens. Environ.* **1989**, *30*, 43–54. [CrossRef]
42. Ceccato, P.; Flasse, S.; Tarantola, S.; Jacquemoud, S.; Grégoire, J.M. Detecting vegetation leaf water content using reflectance in the optical domain. *Remote Sens. Environ.* **2001**, *77*, 22–33. [CrossRef]
43. Seelig, H.D.; Hoehn, A.; Stodieck, L.S.; Klaus, D.M.; Iii, W.W.A.; Emery, W.J. The assessment of leaf water content using leaf reflectance ratios in the visible, near-, and short-wave-infrared. *Int. J. Remote Sens.* **2008**, *29*, 3701–3713. [CrossRef]